Analysis of the binding sites of vitamin D 1α-hydroxylase (CYP27B1) and vitamin D 24-hydroxylase (CYP24A1) for the design of selective CYP24A1 inhibitors: homology modelling, molecular dynamics simulations and identification of key binding requirements

Ismail M. Taban,[a] Jinge Zhu,[b] Hector F. DeLuca[b] and Claire Simons[a*]

[a]Medicinal Chemistry, School of Pharmacy & Pharmaceutical Sciences, Cardiff University, King Edward VII Avenue, Cardiff CF10 3NB, UK; [b]Department of Biochemistry, University of Wisconsin-Madison, 433 Babcock Drive, Madison, WI 53706-1544, USA.

Corresponding author: Tel.: +44 (0) 2920 876307; fax: +44 (0) 2920 874149.

E-mail address: simonsc@cardiff.ac.uk (C. Simons)

Abstract

A homology model of human CYP27B1 was built using MOE and ith further optimisation by molecular dynamics simulations of the hCYP27B1 homology model and a hCYP27B1-SDZ-88357 complex. Docking results from the hCYP27B1-SDZ-88357 complex showed amino acids Arg107, Asn387 and Asp320 have an important role in binding interaction, with Asp320 part of the important acid - alcohol pair situated in the I-helix with the conserved sequence (A/G) GX (E/D) (T/S), which assumes an essential role in the binding of an oxygen molecule for catalysis. Additional docking experiments with selective hCYP27B1 or hCYP24A1 inhibitors using both the hCYP27B1 model and a triple mutant hCYP24A1 model provided further support for the importance of H-bonding interactions with the three identified active site amino acids. To confirm the role of Arg107, Asn387 and Asp320 in the active site of hCYP27B1 compounds were designed that would form H-bonding interactions, as determined from docking experiments with hCYP27B1 model. Subsequent synthesis and CYP24A1 and CYP27B1 enzyme assays of the designed compounds **1a** and **1b** showed a ~ 5-fold selectivity for CYP27B1 confirming the importance of Asp320 in particular and also Asn387 and Arg107 as important amino acids for CYP27B1 inhibitory activity.

Keywords

Vitamin D 1α-hydroxylase (CYP27B1); vitamin D 24-hydroxylase (CYP24A1); molecular modelling; molecular dynamics simulations; enzyme assays; drug synthesis.

1. Introduction

Calcitriol (1,25-dihydroxyvitamin D3) is the biologically active form of vitamin D, with deficiency of calcitriol in human linked to defects in bone formation and mineralisation, for example, rickets in children and osteomalacia in adults[1]. CYP27B1 (vitamin D 1α–hydroxylase), which is expressed primarily in the kidney[2] but is also found in other organs,[3] produces calcitriol by 1α-hydroxylation of 25-hydroxyvitamin D3 (Figure 1).

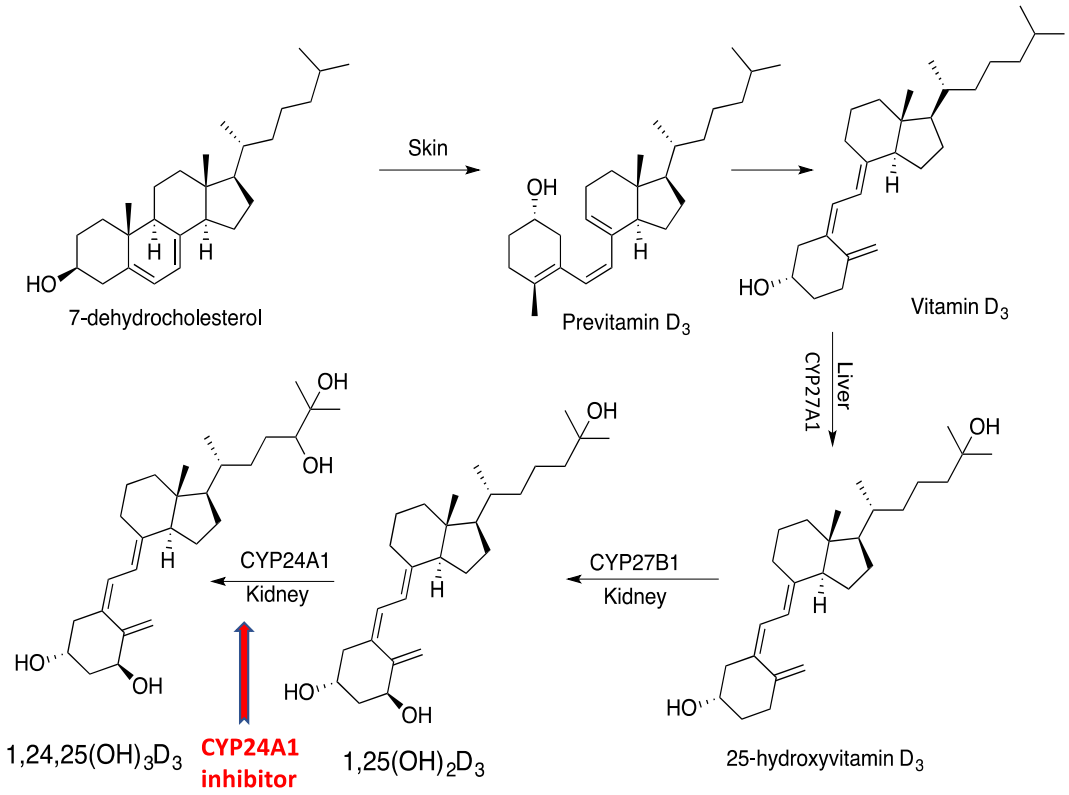

Figure 1. Vitamin D metabolic pathway

Calcitriol subsequently binds to the vitamin D receptor (VDR) to enhance production of target genes[4,5]. Calcitriol is subject to metabolic transformation to inactive polar metabolites by the action of CYP24A1 (vitamin D 24-hydroxylase). Under normal conditions levels of CYP27B1 and CYP24A1, and therefore the levels of calcitriol, are tightly controlled through the action of parathyroid hormone and fibroblast growth factor-23[6,7]. However, increased levels of CYP24A1 have been observed in a number of human cancers including breast[8], colon[9], prostate[10] and skin

cancers[11], directly correlating with a reduction in circulating calcitriol. To enhance circulating levels of the biologically active form of vitamin D, CYP24A1 inhibitors have been developed[12-19] and, although potent inhibitors with IC_{50} values in the nanomolar range have been described, one of the biggest challenges has been designing inhibitors selective for CYP24A1 over CYP27B1. A few azole inhibitors with good selectivity have been described, notably (*R*)-VID400[12] which is ~ 40-fold more selective for CYP24A1 compared with CYP27B1 and the SDZ compounds, SDZ-88357[12] and SDZ-285082[13], which are ~ 166-fold and 47-fold respectively more selective for CYP27B1 over CYP24A1 (Fig. 2).

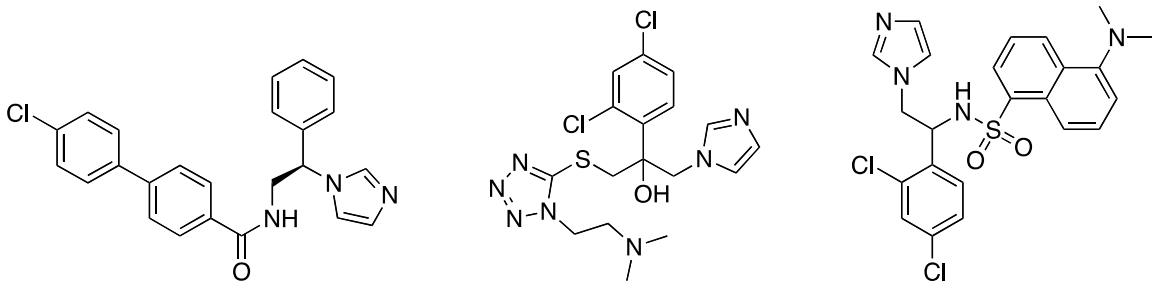

(*R*)-VID400	**SDZ-88357**	**SDZ-285082**
CYP24A1 IC_{50} 15.2 nM	CYP24A1 IC_{50} >10 μM	CYP24A1 IC_{50} 4.48 μM
CYP27B1 IC_{50} 616.1 nM	CYP27B1 IC_{50} 60.2 nM	CYP27B1 IC_{50} 95.2 nM

Figure 2. CYP24A1 and CYP27B1 selective azole inhibitors

To date crystal structures for human CYP24A1 (hCYP24A1) and human CYP27B1 (hCYP27B1) have not been resolved. A model of hCYP24A1 using the rat CYP24A1 (rCYP24A1) crystal structure as a template has previously been described by our group[14,20]. To assist in the design of a selective CYP24A1 inhibitor, a human hCYP27B1 homology model was required in order to analyse any differences between active site architecture and binding interactions of the two enzymes. A hCYP27B1 hybrid homology model, built by combining models generated from rCYP24A1 and hCYP11A1 crystal structures as templates, has been described by Zalewski *et al*[21] in their investigation of mutations in hCYP27B1 related to vitamin D dependent rickets type I. In a

similar manner suitable templates were identified and homology models were generated for our research but with the focus on active site binding/architecture for the purpose of drug design.

2. Results and discussion

2.1 Generation of the hCYP27B1 homology model

Using the UniProt KB/TrEMBL server (ExPASy)[22] the complete human CYP27B1 protein sequence (entry number O15528), composed of 508 amino acids, was selected. A protein-protein BLAST[23] (ncbi) search was run against the Protein Databank (PDB)[24] to identify homologous crystal structures. The most homologous templates were rCYP24A1 and hCYP11A1 with 33% sequence identity, however the rCYP24A1 template had greater sequence coverage, higher BLAST score and E-value (Table 1).

Table 1 The first four hits in the human CYP27B1 BLAST results

Organism	PDB code	BLAST[a] score	Sequence identity[b]	Sequence identity%	Positive %	Chain length	E-Value
CYP24A1 (rat)	3K9V	263	160/478	33	50	482	$4e^{-82}$
CYP11A1 (human)	3N9Y	254	155/474	33	49	487	$2e^{-78}$
CYP11B2 (human)	4DVQ	197	136/415	33	47	483	$7e^{-57}$
CYP3A4 (human)	1W0E	152	134/494	27	45	485	$4e^{-40}$

[a] The BLAST score for an alignment is calculated by summing the scores for each aligned position and the scores for gaps. [b] (Number of identical residues)/(length of sequence fragment identified by BLAST-P).

Clustal Omega 1.2.2[25] was used to align the preferred template sequences and the query sequence of hCYP27B1 (Fig. 3). Conservation was clearly observed between most of the residues of the query sequence and the closely related templates in the active site region, which encompasses the haem binding domain typically sandwiched between helix L on the side of the haem proximal to the surface of the protein and helix I in the inside of the protein as well as the important acid-alcohol pair situated in the I-helix with the conserved sequence (A/G) GX (E/D) (T/S) (Fig. 3).

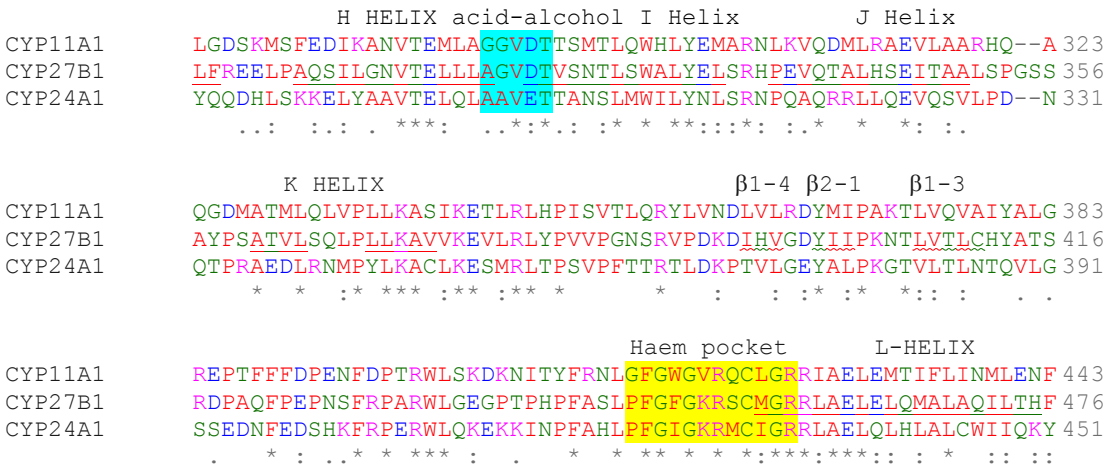

Figure 3. CLUSTAL alignment of the active site region of the hCYP27B1 protein sequence against rCYP24A1 and hCYP11A1 human protein sequences. *Asterisk* identical residues, *colon* highly conserved residues, *dot* residues are somewhat similar. The residues are colored according to their chemical properties: *red* small hydrophobic (AVFPMILWY), *blue* acidic (DE), *magenta* basic (RHK), *green* hydroxyl + amine + basic (STYHCNGQ)

Homology models using both rCYP24A1 and hCYP11A1 were generated using MOE software and based on validation results using Ramachandran plots[26], Verify 3D[27] and ProSA[28], as well as BLAST analysis and consideration of template enzyme function, the homology model from rCYP24A1 as template was chosen for further optimisation and docking studies.

2.2 Molecular dynamics studies

Further optimisation of the active site architecture was achieved by molecular dynamics simulations, using the Desmond programme of Maestro[29], carried out at two different temperatures, 300 K and 312 K. Molecular dynamics simulation at 300 K and 312 K represent normal body temperature and elevated body temperature.

2.2.1 Molecular dynamics of hCYP27B1 model at 300K

The RMSD values of the backbone atoms were plotted as a time-dependent function of the molecular dynamics simulation. The outcomes support the CYP27B1 model structure, as they show time dependence of constant RMSD (Å) of the backbone atoms throughout the whole simulation

process. This demonstrates that the model achieved equilibrium after some initial fluctuations. The chart plainly shows that there is an adjustment in the RMSD from 0.9 Å to 2.4 Å and that it reached 2.02 Å at 1.39 ns and then declined to 1.83 Å at 1.83 ns, but after that, it reached a plateau from 2.25 ns (Figure 4A and 4B).

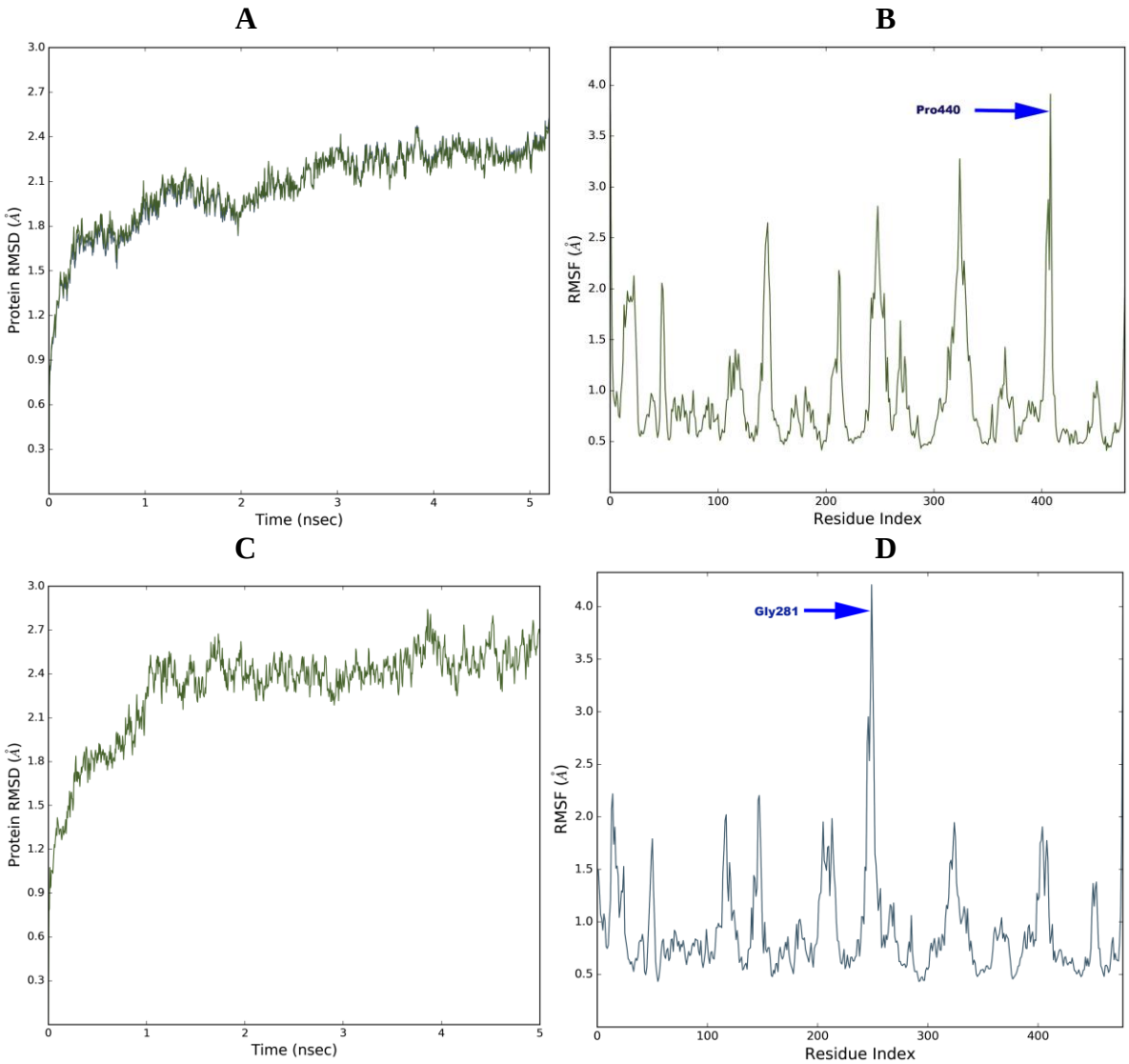

Figure 4. (**A**) Time-dependent RMSD (Å) of backbone atoms of the CYP27B1 model at 300 K (**B**) Root mean square fluctuation (RMSF) showed the differences of structural behaviours and flexibilities in each residue for the CYP27B1 model; the amino acid residue (Pro440) was shown to be highly fluctuated. (**C**) Time-dependent RMSD (Å) of backbone atoms of the CYP27B1 model at 312 K (**D**) Root mean square fluctuation (RMSF) showed the differences of structural behaviours and flexibilities in each residue for the CYP27B1 model; the amino acid residue (Gly281) was shown to be highly fluctuated.

2.2.2 Molecular dynamics of hCYP27B1 model at 312 K

The RMSD of the backbone atom values for CYP27B1 at 312 K simulations were not much different from the simulations at 300 K. However, the graph clearly indicates that there is a change in the RMSD from 0.9 Å to 2.5 Å, and it reaches a plateau from 2.48 ns (Fig. 4C and 4D). Overall, it can be said that there is no significant difference in structure during molecular dynamics simulations at temperatures 300 K and 312 K. This means that at 312 K, the model still has activity, and no structural damage has occurred.

To validate the optimised hCYP27B1 model structure, Ramachandran plots were run before as well as after molecular dynamics simulation. The number of outlier amino acids after molecular dynamics was 5 (1.1%) compared with 12 (2.5%) amino acid outliers prior to molecular dynamics. The five outliers were found to be in the outer regions of the protein within loops, which are very difficult to model, and away from the active site.

2.2.3. Molecular dynamic simulation of the hCYP27B1-SDZ-88357 complex at 300 K

A molecular dynamics simulation of the hCYP27B1 model complexed with the CYP27B1 selective inhibitor SDZ-88357 was run for 50 ns. The RMSD changed from 1.37 Å at zero time to 3.57 Å at 33.44 ns; then the protein was equilibrated with no evident RMSD fluctuations observed after 33.44 ns. Ligand RMSD (right Y- axis, Fig. 5) demonstrates how stable the ligand is regarding the protein and its binding pocket. The red line indicates the RMSD of a ligand when the hCYP27B1-SDZ-88357 complex is initially aligned on the protein backbone of the reference and then the RMSD of the ligand heavy atoms is measured. A pink line (Lig fit Lig) indicates the RMSD of a ligand that is aligned and measured just on its reference conformation (Fig. 5). This RMSD value measures the internal fluctuations of the ligand atoms.

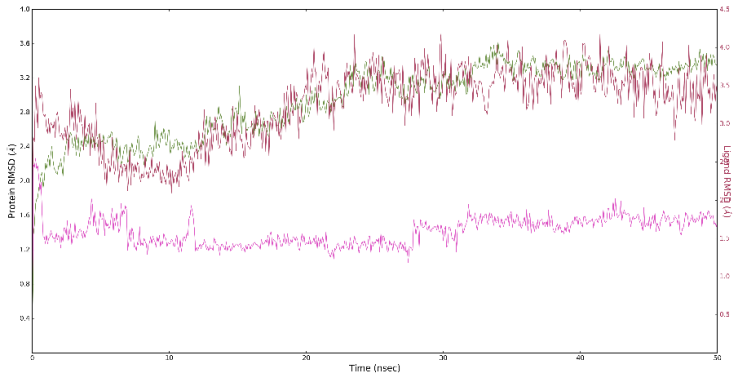

Figure 5: Protein and ligand root mean square fluctuation (RMSF) of the hCYP27B1-SDZ-88357 complex.

Protein interactions with the ligand were checked throughout the simulation and interactions are ordered by their type; specifically hydrogen bonds, hydrophobic, ionic, and water bridges (Fig. 6).

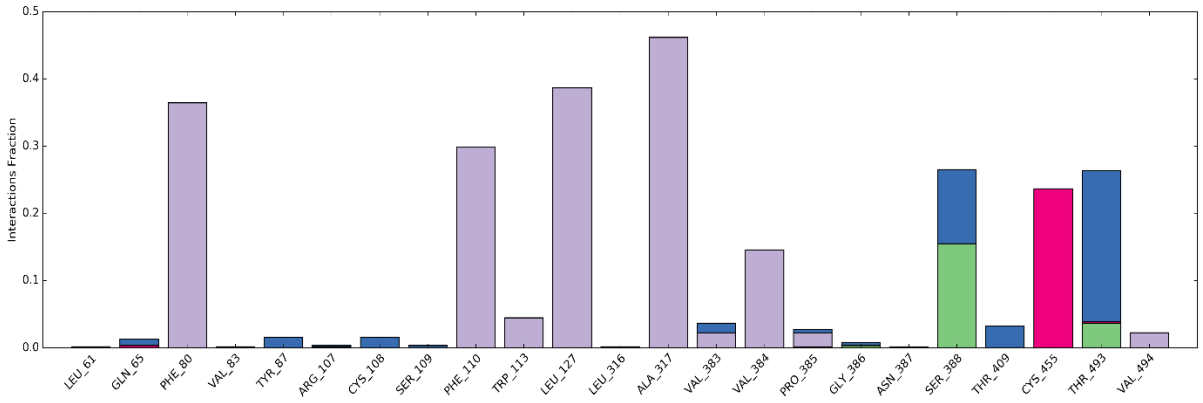

Figure 6. Illustration of protein interactions with the ligand. The red column means ionic bond, green column a hydrogen bond, blue column water bridges, and a purple column a hydrophobic bond. The stacked bar charts are normalised over the course of the trajectory: for example, a value of 0.5 suggests that for 50% of the simulation time, the specific interaction is maintained.

Interaction between the nitrogen lone pair of the tetrazole ring of SDZ-88357 and the haem iron at a distance of 2.25 Å was observed with hydrophobic interactions with amino acid residues in the active site (Phe110, Leu127, Pro385 and Gly386) (Fig. 7). In addition, SDZ-88357 was observed making three additional hydrogen bonds with amino acids Arg107, Asn387 and Asp320.

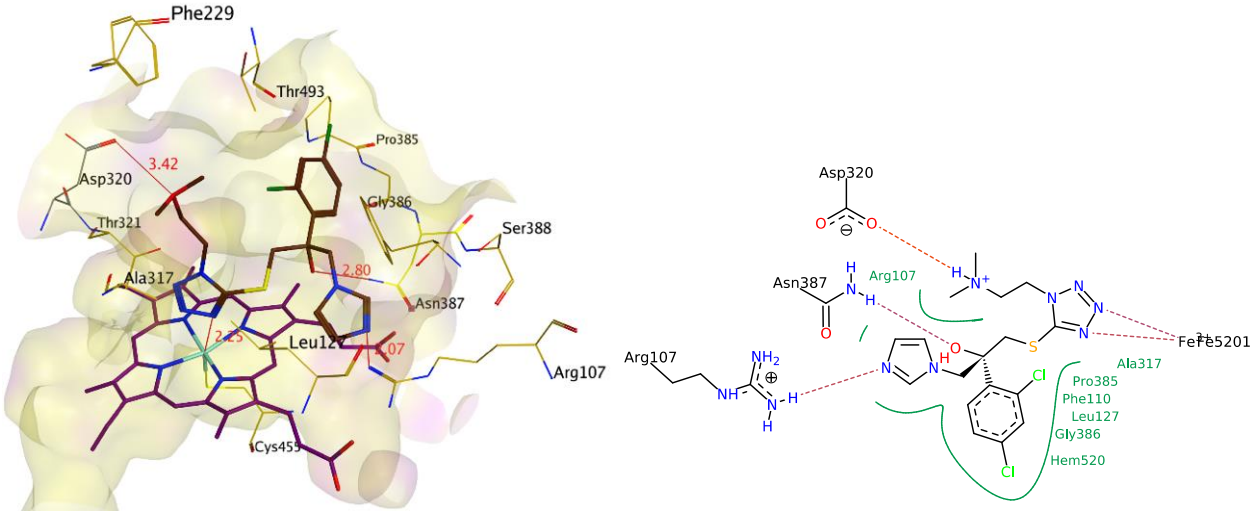

Figure 7. 3D and 2D images showing interactions between SDZ-88357 and hCYP27B1 active site

Asp320 is included in the acid - alcohol pair situated in the I-helix with the conserved sequence (A/G) GX (E/D) (T/S), which assumes an essential role in the binding of an oxygen molecule for catalysis. In contrast (*R*)-VID400, a selective CYP24A1 inhibitor, on docking in the hCYP27B1 optimised model was positioned unfavourably at too great a distance from the haem iron (4.16 Å) to form an interaction with the imidazole ring of this CYP24A1 inhibitor, and no H-bonding interaction formed with the hydrophobic 4-chlorobiphenyl side chain (Fig. 8A and B). However SDZ-285082 docked favourably with hydrogen bonding interactions with Arg107 and Asn387 as observed for SDZ-88357 (Fig. 8C and D).

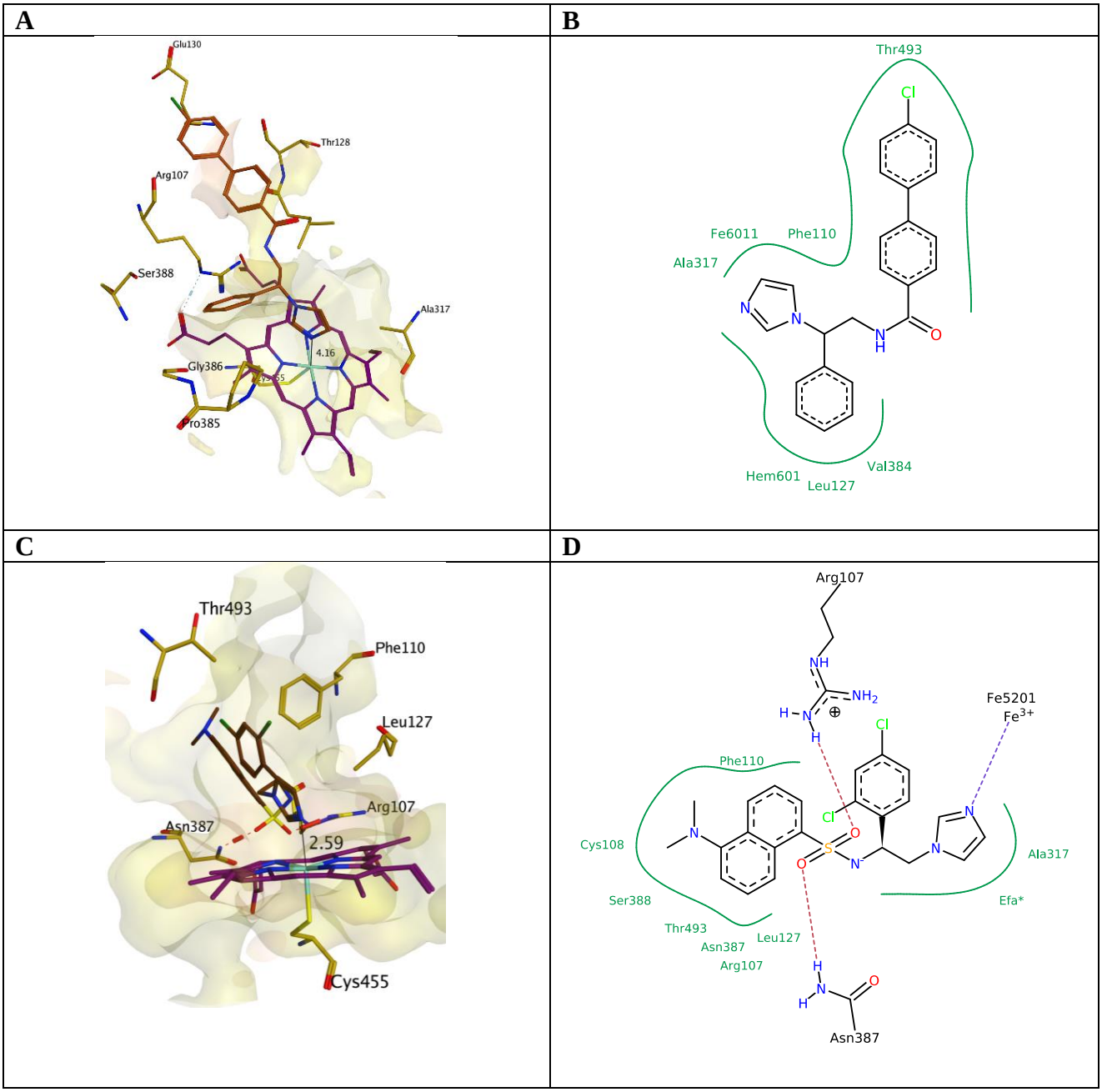

Figure 8. (**A**) 3D image of (*R*)-VID400 in CYP27B1 active site (B) 2D image (*R*)-VID400 in CYP27B1 active site (C) 3D image of SDZ-285092 in CYP27B1 active site (B) 2D image SDZ-285092 in CYP27B1 active site

2.2.4 Docking of SDZ-88357 in the hCYP24A1 model and a triple mutant hCYP24A1 model

Schuster *et al*.[4] showed that SDZ-88357 was a very weak inhibitor of the CYP24A1 enzyme (> 10 μM). Docking results with our hCYP24A1 model concur with experimental data with the distance between the nitrogen lone pair of tetrazole and the haem iron at a distance of 5.56 Å, that is, too far a distance for interaction.

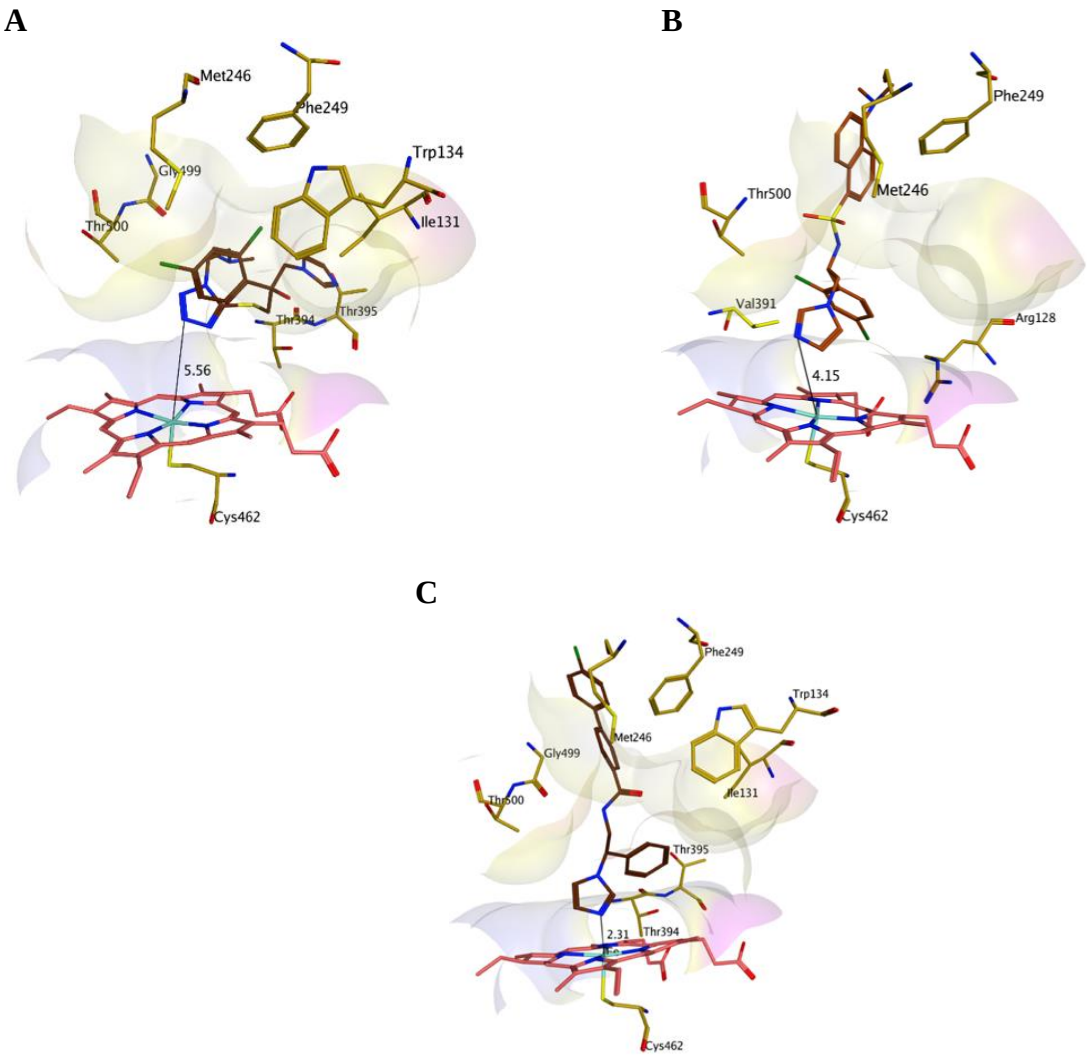

Figure 9. Docking of (**A**) SDZ-88357 and (**B**) SDZ-285082 and (**C**) (*R*)-VID400 in the hCYP24A1 model active site

There were multiple hydrophobic interactions between the SDZ-88357 with amino acid residues in the active site (Arg128, Leu129, Ile131, Trp134, Leu148, Met246, Phe249, Leu325, ala326, Val391, Pro392, Phe393, Thr395, His497, Gly499 and Thr500) (Fig. 9A) but no hydrogen bonding interactions within the hCYP24A1 hydrophobic active site cavity. SDZ-285082 docked in a similar manner and was also positioned too far from the haem iron (4.15Å) to interact (Fig. 9B). This was in contrast with (*R*)-VID400 with the distance between the nitrogen of imidazole and the haem iron observed as 2.31Å (Fig. 9C).

To explore the potential importance of H-bonding interactions in the inhibitory activity and selectivity of SDZ-88357 in hCYP27B1, a computational triple hCYP24A1 mutant was generated using MOE software[30]. After alignment of the hCYP24A1 and hCYP27B1 3D models, amino acids of hCYP24A1 that were comparable in position with Arg107, Asp320 and Asn387 were identified and mutated as follows: L148A, H497R and G499N. Subsequent docking of SDZ-88357 in the triple mutant hCYP24A1 model resulted in favourable interaction with the haem (distance 2.38 Å) and additional hydrogen bonding interactions (Figure 10).

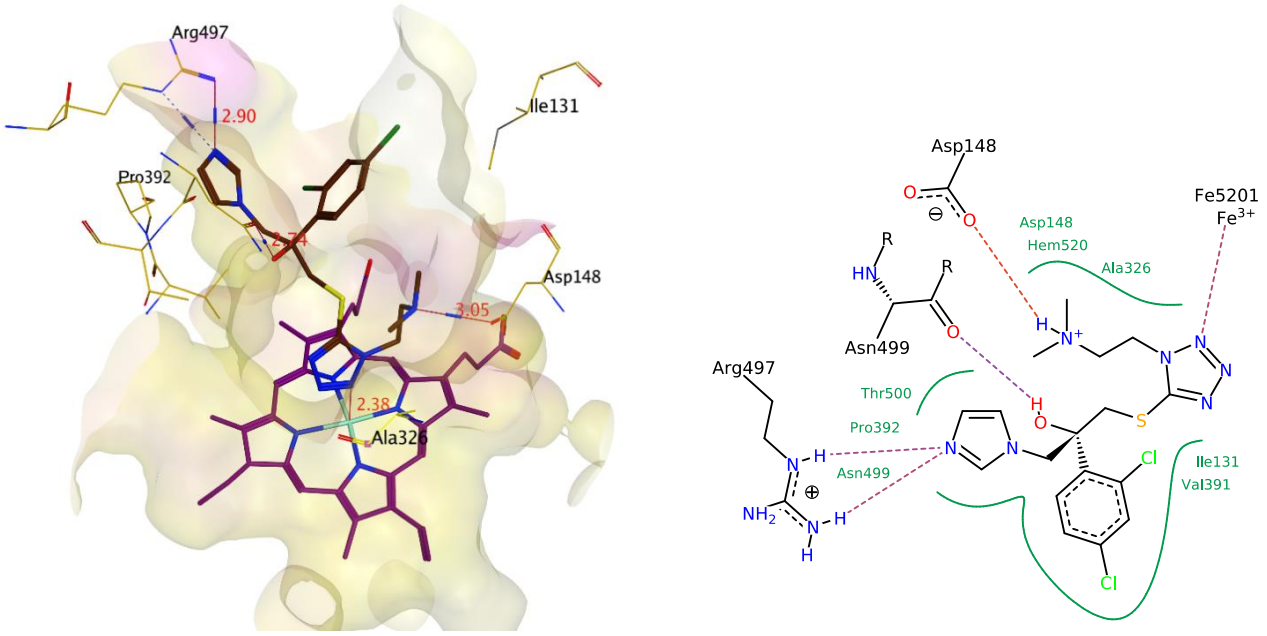

Figure 10: 3D and 2D docking images of SDZ-88357 in the triple mutant hCYP24A1 active site

From these computational studies the requirement for CYP24A1 selectivity is linked with hydrophobic pharmacophores, whilst CYP27B1 selectivity is linked with pharmacophores capable

of hydrogen and/or ionic bonding interactions. To further confirm this compounds containing the pharmacophores necessary for haem binding and hydrogen/ionic bonding interactions combined with the classic T- or Y-shaped inhibitor shape were required.

2.3 Design and synthesis of hCYP27B1 inhibitors

With the new findings regarding hCYP24A1 vs hCYP27B1 requirements for selectivity, further evaluation of optimal pharmacophores was reconsidered and through combining key binding requirements (haem binding, H-bonding functional group) the 4,4'-((3/4-(pyridin-4-ylmethoxy)phenyl)methylene)bis(3-methyl-1*H*-pyrazol-5-ol) structures (**1a** and **1b**) were designed to explore binding/inhibition profiles. **1a** and **1b** displayed interesting results in the docking experiments with hCYP24A1 and hCYP27B1 and could be generated using a short efficient synthetic route.

A

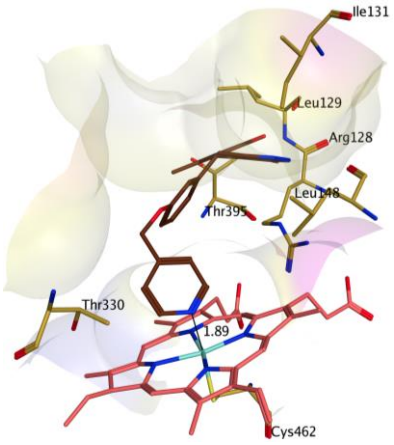

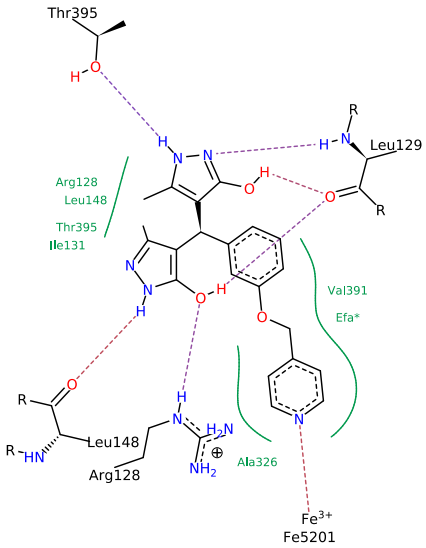

B

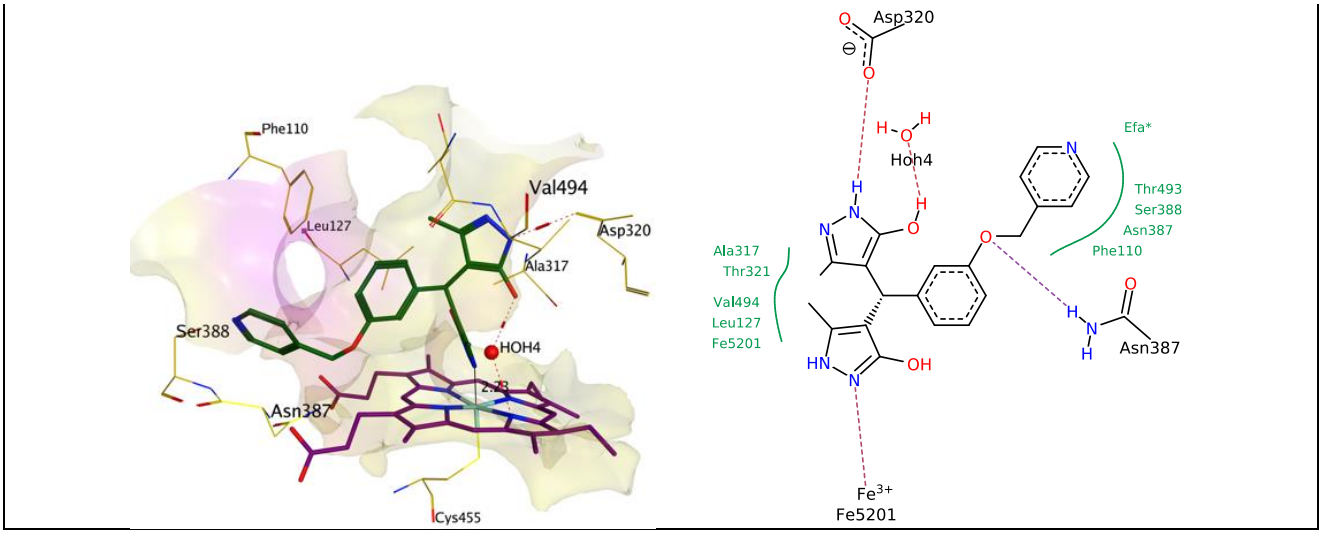

Figure 11: 3D and 2D docking images of **1a** in the (**A**) hCYP24A1 model, and (**B**) hCYP27B1 model.

When **1a** and **1b** were docked in the hCYP24A1 model, interaction with the haem iron was through the pyridyl nitrogen with hydrogen bonding with Arg128, Leu129, Glu130, Leu148 and Thr395 as illustrated in Figure 11A. The docking would predict CYP24A1 inhibitory activity, with the longer pyridin-4-ylmethoxy group allowing close binding with the haem, however the hydrophilic functional groups with resulting hydrogen bonding would suggest CYP27B1 inhibitory activity. Docking of **1a** and **1b** in the hCYP27B1 model did indicate good fit, hydrogen bonding interactions (Asp320 and Asn387, identified as important for CYP27B1 inhibitory activity) and haem binding, although in the hCYP27B1 model haem binding was optimal through a pyrazole nitrogen (Fig. 11B).

The designed compounds (**1**) were readily obtained in two steps. The 3/4-(pyridine-4-ylmethoxy)benzaldehydes (**3**) were prepared as previously described[31] on reaction of 3/4-hydroxybenzaldehyde (**2**) with potassium carbonate and 4-(chloromethyl)pyridine hydrochloride. Reaction of the 3/4-(pyridine-4-ylmethoxy)benzaldehydes (**3**) with hydrazine hydrate and ethyl acetoacetate, employing 2-hydroxy ethylammonium propionate (2-HEAP[32]) as the catalyst, gave the required 4,4'-((3/4-(pyridin-4-ylmethoxy)phenyl)methylene)bis(3-methyl-1*H*-pyrazol-5-ol) derivatives (**1a** and **1b**) (Scheme 1).

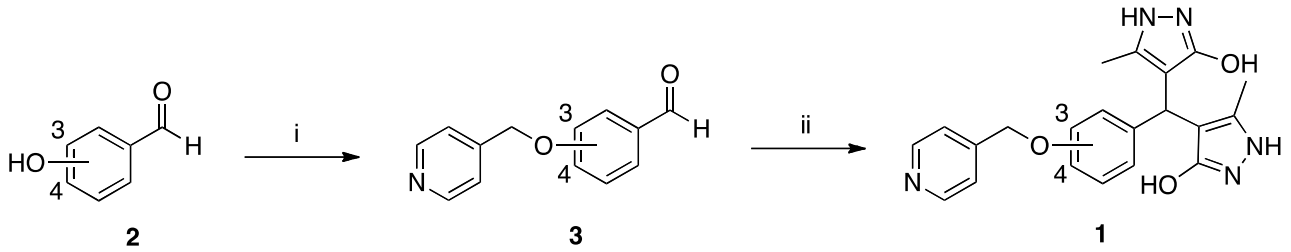

Scheme 1. Reagents and conditions: (i) K_2CO_3, DMF, 4-(chloromethyl)pyridine hydrochloride, 80 ^oC, 7h (ii) H_2NNH_2, ethyl acetoacetate, 2-HEAP, 90 ^oC, 1 h.

2.4 CYP24A1 and CYP27B1 enzymatic assay

The CYP24A1 enzymatic assay followed methodology previously described[33]. In short, human CYP24A1 with an N-terminal fusion to maltose binding protein (MBP) was overexpressed in Escherichia coli and purified to homogeneity. The hydrolase activity was reconstituted *in vitro*, and the resulting cell-free assay system was applied in the screening of the compounds to measure IC_{50} The inhibition assay of CYP27B1 was similar to the CYP24A1 assay as previously described[33], and the resulting cell-free assay system was applied in the screening of the compounds to measure IC_{50}. The main difference between **1a** and **1b** was changing the position of the ether group from the para position to the meta position on the phenyl ring, but it resulted in no notable difference in CYP24A1 or CYP27B1 inhibitory activity. **1a** and **1b** displayed modest CYP24A1 inhibitory activity of 2.5 and 2.6 □M respectively compared with the standard ketoconazole (KTZ, IC_{50} 0.5 μM), however as expected from docking they displayed potent CYP27B1 inhibitory activity comparable with KTZ (IC_{50} 0.34 μM) with IC_{50} 0.57 and 0.41 μM respectively.

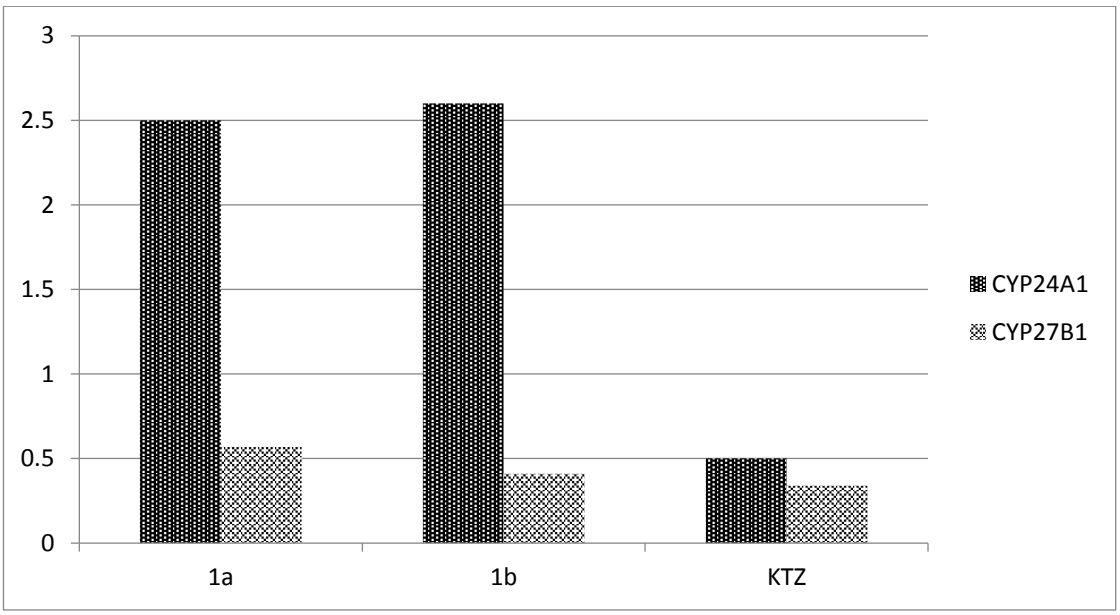

Figure 12. hCYP24A1 and hCYP27B1 inhibitory activity

1a and **1b** have selectivity for CYP27B1 that is ~ 5-fold greater than CYP24A1 (Fig. 12). The selectivity of **1a** and **1b** can be rationalised by better fit and binding in the hCYP27B1 active site, where the pyrazole ring interacted with the haem iron in addition to formation of hydrogen bonds with Asp320 and Asn387, which are important amino acids in hCYP27B1.

3. Conclusions

A homology model of CYP27B1 was built using MOE and was evaluated for stereochemical and amino acid environment quality using appropriate programmes, with further optimisation of the active site architecture achieved by molecular dynamics simulations. Understanding protein-ligand interactions is essential for designing more selective and potent CYP24A1 inhibitors. This work uses a combination of homology modelling, molecular dynamics simulations, and molecular docking to understand the binding requirements of the hCYP27B1 enzyme. Docking results from the hCYP27B1-SDZ-88357 complex showed amino acids Arg107, Asn387 and Asp320 have an important role in binding interaction. Asp320 was part of the αI helix for the CYP27B1 model, which covers the haem binding site and contains SRS-4, and plays a key role in orientating the

ligand at the active site by electrostatic interactions. Asp320 has the important acid - alcohol pair situated in the I-helix with the conserved sequence (A/G) GX (E/D) (T/S), which assumes an essential role in the binding of an oxygen molecule for catalysis. The main strategy that can be used to build inhibitors selective for CYP24A1 over CYP27B1, is to design compound unable to form hydrogen bonding interactions with CYP27B1 especially with Arg107, Asn387 and Asp320. To confirm the role of Arg107, Asn387 and Asp320 in the active site of hCYP27B1 compounds were designed that would form hydrogen bonding interactions, as determined from docking experiments with hCYP27B1. Subsequent synthesis and CYP24A1 and CYP27B1 enzyme assays of the designed compounds **1a** and **1b** showed a ~ 5-fold selectivity for CYP27B1 confirming the importance of Asp320 in particular and also Asn387 and Arg107 as important amino acids for CYP27B1 inhibitory activity.

Although additional H-bonds can improve binding and potentially inhibitory activity of hCYP24A1 this is at the expense of selectivity. Incorporating larger hydrophic pharmacophores capable of filling the active site cavity and formation of multiple hydrophic interactions with active site amino acids would result in CYP24A1 inhibitory activity and crucially selectivity with respect to CYP27B1.

4. Experimental

4.1 General Experimental

$1,25(OH)_2D_3$ and $25(OH)D_3$ were purchased from SAFC-Pharma (Madison, WI). Human MBP-CYP24A1, CYP27B1, bovine adrenodoxin (Adx), and adrenodoxin reductase (AdR) were purified as described previously[33]. All solvents used for chromatography were HPLC grade from Fisher Scientific (UK).

^1H and ^{13}C NMR spectra were recorded with a Bruker Avance DPX500 spectrometer operating at 500 and 125 MHz, with Me_4Si as internal standard. Mass spectra and microanalysis were determined by the MEDAC (Chobham, UK). Flash column chromatography was performed with

silica gel 60 (230-400mesh) (Merck) and TLC was carried out on precoated silica plates (kiesel gel 60 F_{254}, BDH). Compounds were visualised by illumination under UV light (254 nm) or by the use of vanillin stain followed by charring on a hotplate. Melting points were determined on an electrothermal instrument and are uncorrected. All solvents were dried prior to use and stored over 4Å molecular sieves, under nitrogen. All compounds were more than 95% pure.

4.2 Molecular modelling

4.2.1 Homology search

The protein sequence for hCYP27B1 was obtained from the ExPASy proteomics server at the Swiss Bioinformatics Institute[22]. The enzyme sequence for the hCYP27B1 has the Uniprot identifier O15528 and is composed of 508 amino acids. A homology search was performed using protein BLAST accessible from the NCBI website[23], which was used to align the query sequence (hCYP27B1) against the sequences in the protein data bank[24] and thus the close homologous proteins were identified. The alignment parameters and the thresholds, which were used for screening expected homologues, were used with their default values and BLOSUM62 comparison matrix.

4.2.2. 3D model building

The molecular experiments were performed using Molecular Operating Environment (MOE) 2014.0901 molecular modeling software[30]. Homology models were built using MOE-Homology using AMBER99 forcefield[34], which uses a dictionary to set the partial charges of atoms in amino acids. The final homology model was constructed using rCYP24A1 (3K9V-A) and hCYP11A1 (3N9Y) crystal structure. Ten intermediate models were generated and the final model was taken as the Cartesian average of all the intermediate models. All minimisations were performed until RMSD gradient of 0.05 kcal $mol^{-1}Å^{-1}$ with the specified forcefield and partial charges automatically calculated.

4.2.3. Model validation

Stereochemical quality of the polypeptide backbone and side chains was evaluated using Ramachandran plots obtained from the RAMPAGE server[26]. The compatibility of the 3D model with its own amino acid 1D sequence was examined using Verify 3D[27]. The ProSA server[28] was used to check defaults in the three dimensional protein structure based on statistical analysis. Validation data from the templates (3K9V-A and 3N9Y) was used as the baseline to evaluate the model.

4.2.4. Molecular dynamics simulation

A molecular dynamics simulation was run on the hCYP27B1 model alone and the CYP27B1 model in complex with SDZ-88357. Both PDB files were first optimised with protein preparation wizard in Maestro, version 11.0.015[29] by assigning bond orders, adding hydrogen, and correcting incorrect bond types. A default quick relaxation protocol was used to minimise the MD systems with the Desmond program[29]. In Desmond, the volume of space in which the simulation takes place (the global cell) is built up by regular 3D simulation boxes, which was utilised as part in this system for protein interactions. The orthorhombic water box (volume = 501882 $Å^3$) allowed for a 10 Å buffer region between protein atoms and box sides. Overlapping water molecules were deleted, and the systems were neutralised with Na^+ ions and salt concentration 0.15 M. Force-field parameters for the CYP27B1 model and the CYP27B1 model-SDZ-88357 complex were assigned using the OPLS_ 2005 force-field, that is, a 5 ns or 50 ns molecular dynamic run in the NPT ensemble (T = 300 K) at a constant pressure of 1 bar. Energy and trajectory atomic coordinate data were recorded at each 1.2 ns. Molecular dynamics simulation for drug design is ideally conducted at a temperature range of 300 -314 K. In this study, molecular dynamics simulations were done at 300 K and 312 K.

4.2.5. Docking

Docking studies were performed using LeadIT2.1.2 docking program by BioSolve.IT[35]. The important amino acid residues of the active pocket (Gln82, Ile131, Trp134, Met246, Ala326,

Glu329, Thr330, Val391, Phe393, Thr394, Ser498, Gly499, Tyr500)[20] were selected and then the selection was extended to 12 Å in order to include in the docking site the haem iron region and the access tunnel to the catalytic site. A ligands database in mol2 format, prepared using MOE[30], was used as input for the docking calculations. The iron atom of the catalytic site was set as essential pharmacophoric feature. Ligand docking was performed using the default values and no water molecules were considered. Ten output solutions were obtained from each compound and visual inspection in MOE was used to identify the interaction between ligand and protein.

4.3. Chemistry

4.3.1. General procedure for the preparation 4,4'-((4/3-(Pyridin-4-ylmethoxy)phenyl)methylene)bis(3-methyl-1H-pyrazol-5-ol) (1a) and (1b)

Hydrazine monohydrate (0.18 ml, 1.7 mmol) was mixed with ethyl acetoacetate (0.22 mL, 1.7 mmol). Then 2-hydroxy ethylammonium propionate (2-HEAP) (0.07 g, 0.5 mmol) was stirred under solvent free conditions for 40 min. Then, the 4-(pyridin-4-ylmethoxy)benzaldehyde[31] (0.30 g, 1.4 mmol) (**3a**) or the 4-(pyridin-3-ylmethoxy)benzaldehyde[31] (0.40 g, 1.9 mmol) (**3b**) was added and the reaction mixture heated at 90 ℃ for 1 h. After completion, the reaction was cooled to room temperature, where upon it solidified. The pure product was obtained from this solid by recrystallisation with methanol[7].

*4.3.1.1. 4,4'-((4-(Pyridin-4-ylmethoxy)phenyl)methylene)bis(3-methyl-1H-pyrazol-5-ol) (**1a**).*

Tan crystalline solid obtained after recrystallization from methanol. Yield: 36%; Rf 0.34 (CH_2Cl_2-CH_3OH 9: 1 v/v); mp 194 - 198 °C; ^{1}H NMR ($CDCl_3$): δ 8.69 (d, *J* = 6.0, 2H, Ar), 7.41 (d, *J* = 6 Hz, 2H, Ar), 7.16 (t, *J* = 8.0 Hz, 2H, Ar), 6.76 (m, 2H, Ar), 5.08 (s, 2H, CH_2), 4.47 (s, 1H, CH), 2.06 (s, 6H, $2CH_3$). ^{13}C NMR ($CDCl_3$ δ: 158.2 (C), 150.1 (CH, Ar), 146.7, 145.8, 146.3 (8 × C), 129.3, 122.4, 121.0, 115.3, 123.4, 111.4 (6 × CH, Ar), 102.4 (CH, Ar), 68.0 (CH_2), 35.4 (CH), 10.8 (2 × CH_3). LRMS (ES-TOF) m/z: 392 $[M + H]^+$. HRMS (ES-TOF) Calculated mass: 392.1717 $[M + H]^+$, measured mass: 392.1720 $[M + H]^+$.

*4.3.1.2. 4,4'-((3-(Pyridin-4-ylmethoxy)phenyl)methylene)bis(3-methyl-1H-pyrazol-5-ol) (**1b**)*

Tan crystalline solid obtained after recrystallization from methanol. Yield: 25%; Rf 0.75 (EtOAc-CH_3OH 6: 1 v/v); mp 264 - 268 °C; ^1H NMR ($CDCl_3$): δ 8.55 (d, J = 5.7 Hz, 2H, Ar), 7.40 (d, J = 5.8 Hz, 2H, Ar), 7.15 (t, J = 8.3 Hz, 1H, Ar), 6.75 (m, 3H, Ar), 5.08 (s, 2H, CH_2), 4.72 (s, 1H, CH), 2.06 (s, 6H, $2CH_3$). ^{13}C NMR ($CDCl_3$) δ: 158.2, 156.2 (2 × C), 150.7, 145.8 (2 × CH, Ar), 145.9, 141.3. 129.2, 128.3, 122.42 (6 × CH, Ar), 121.0, 115.3, 111.4 (7 × C), 67.9 (CH_2), 33.2 (CH), 11.2 (2 × CH_3). LRMS (ES-TOF) m/z: 392 $[M + H]^+$. HRMS (ES-TOF) Calculated mass: 392.1717 $[M + H]^+$, measured mass: 392.1707 $[M + H]^+$.

4.4. Enzymatic assays

Inhibition of hCYP24A1 was performed as previously described[33]. Briefly, reaction mixture containing 0.1 μM each of Adx and AdR, 0.075 μM MBP-CYP24A1, 2.5 μM $1,25(OH)_2D_3$, varying concentrations of inhibitors, and 0.5 mM NADPH was incubated at 37 °C for 25 min in a buffer of 20 mM Tris (pH 7.5) and 125 mM NaCl. All inhibitors were dissolved in ethanol (>10 mM) or DMSO (>50 mM) and further diluted in ethanol to make working stock (<1 mM). The reaction was extracted with CH_2Cl_2 and analysed by HPLC. The IC_{50} values were determined by fitting the relative activity (V/V_0) against the inhibitor concentration [I] using the equation $V/V_0 = IC_{50}/(IC_{50} + [I])$, where V and V_0 are the reaction rates in the presence and absence of inhibitors. The assay for each compound was performed in at least duplicate and in triplicate for compounds with good inhibitory properties. Inhibition assay of hCYP27B1 was performed in a way similar to that of CYP24A1 as previously described[33].

Supplementary material

Supplementary data associated with this article can be found, in the online version, at ……

Clustal analysis; Model validation – Ramachandran, Verify3D, ProSA ; Secondary structure prediction; Synthesis of 2-HEAP and **3a** and **3b**.

Acknowledgements

We acknowledge the Cultural Attaché, Libyan Embassy, London and Misurata University for a PhD scholarship to Ismail M. Taban.

References

(1) Malloy, P.J.; Feldman, D. Genetic disorders and defects in vitamin D action. *Endocrinol. Metab. Clin. North Am.* **2010**, *39*, 333-346.

(2) Zehnder, D.; Bland, R.; Walker, E.A.; Bradwell, A.R.; Howie, A.J.; Hewison, M.; Stewart, P.M. Expression of 25-hydroxyvitamin D3-1alpha-hydroxylase in the human kidney. *J. Am. Soc. Nephrol*. **1999**, *10*, 2465–2473.

(3) Cross H.S. Extrarenal vitamin D hydroxylase expression and activity in normal and malignant cells: modification of expression by epigenetic mechanisms and dietary substances. *Nutr. Rev*. **2007**, *65*, S108-S112.

(4) Bikle, D.D. Vitamin D metabolism, mechanism of action, and clinical applications. *Chem. Biol*. **2014**, *21*, 319-329.

(5) Pike, J.W.; Meyer, M.B.; Bishop, K.A. Regulation of target gene expression by the vitamin D receptor – an update on mechanisms. *Rev. Endocr. Metab. Disord*. **2012**, *13*, 45-55.

(6) de Brito Galvao, J.F.; Nagode, L.A.; Shenck, P.A.; Chew, D.J. Calcitriol, calcidiol, parathyroid hormone, and fibroblast growth factor-23 interactions in chronic kidney disease. *J. Vet. Emerg. Crit. Care* **2013**, *23*, 134-162

(7) DeLuca, H.F. Overview of the general physiologic features and functions of vitamin D. *Am. J. Clin. Nutr*. **2004**, *80*, 1689-1696.

(8) Lopes N.; Sousa, B.; Martins, D.; Gomes, M.; Vieira, D.; Veronese, L.A.; Milanezi, F.; Paredes, J.; Costa, J.L.; Schmitt, F. Alterations in vitamin D signalling and metabolic pathways in breast cancer progression: a study of VDR, CYP27B1 and CYP24A1 expression in benign and malignant breast lesions. *BMC Cancer* **2010**, *10*, 483-492.

(9) Matusiak, D.; Murillo, G.; Carroll, R.E.; Mehta, R.G.; Benya, R.V. Expression of vitamin D receptor and 25-hydroxyvitamin D3-1α-hydroxylase in normal and malignant human colon. *Cancer Epidemiol. Biomark. Prev*. **2005**, *14*, 2370–2376.

(10) Chen, T.C.; Wang, L.; Whitlatch, L.W.; Flanagan, J.N.; Holick, M.F. Prostatic 25-hydroxyvitamin D-1α-hydroxylase and its implication in prostate cancer. *J. Cell. Biochem.* **2003**, *88*, 315–322.

(11) Brożyna, A.A.; Jochymski, C.; Janjetovic, Z.; Jóźwicki, W.; Tuckey, R.C.; Slominski, A.T. CYP24A1 expression inversely correlates with melanoma progression: clinic-pathological studies. *Int. J. Mol. Sci*. **2014**, *15*, 19000-19017.

(12) Schuster, I.; Egger, H.; Bikle, D.; Herzig, G.; Reddy, G.S.; Stuetz, A.; Stuetz, P.; Vorisek, G. Selective inhibition of vitamin D hydroxylase in human keratinocytes. *Steroids* **2001**, *66*, 409-422.

(13) Schuster, I.; Astecker, N.; Egger, H.; Herzig, G.; Reddy, S.; Schuessler, M.; Vorisek, G.; Wachter, C. Inhibitors of vitamin D hydroxylases: mechanistic tools and therapeutic aspects. In: Stolzt, D. V, Ed.; New topics in vitamin D research; Nova Science: New York, 2006; pp 95–96.

(14) Salvo Ferla, S.; Aboraia, A. S.; Brancale, A.; Pepper, C. J.; Zhu, J.; Ochalek, J. T.; DeLuca, H. F.; Simons, C. Small molecule inhibitors of 25-hydroxyvitamin D-24-hydroxylase (CYP24A1): synthesis and biological evaluation. *J. Med. Chem.* **2014**, *57*, 7702–7715.

(15) Salvo Ferla, S.; Gomaa, S.M.S.; Brancale, A.; Zhu, J.; Ochalek, J. T.; DeLuca, H. F.; Simons, C. Novel styryl-indoles as small molecule inhibitors of 25-hydroxyvitamin D-24-hydroxylase (CYP24A1): synthesis and biological evaluation. *Eur. J. Med. Chem*. **2014**, *87*, 39-51.

(16) Aboraia, A.S.; Yee, S.W.; Gomaa, M.S.; Shah, N.; Robotham, A.C.; Makowski, B.; Prosser, D.; Brancale, A.; Jones, G.; Simons, C. Synthesis and CYP24A1 inhibitory activity of *N*-(2-(1*H*-imidazol-1-yl)-2-phenylethyl)arylamides. *Bioorg. Med. Chem.*, **2010**, *18*, 4939-4946.

(17) Taban, I.M.; Zhu, Z.; DeLuca, H.F.; Simons, C. Synthesis, molecular modelling and CYP24A1 inhibitory activity of novel of (*E*)-N-(2-(1*H*-imidazol-1-yl)-2-(phenylethyl)-3/4-styrylbenzamides. *Bioorg. Med.Chem*. **2017**, DOI: 10.1016/j.bmc.2017.05.055

(18) Chiellini, G.; Rapposelli, S.; Zhu, J.; Massarelli, I.; Saraceno, M.; Bianucci, A. M.; Plum, L. A.; Clagett-Dame, M.; DeLuca, H. F. Synthesis and biological activities of vitamin D-like inhibitors of CYP24 hydroxylase. *Steroids* **2012**, *77*, 212−223.

(19) Kahraman, M.; Sinishtaj, S.; Dolan, P. M.; Kensler, T. W.; Peleg, S.; Saha, U.; Chuang, S. S.; Bernstein, G.; Korczak, B.; Posner, G. H. Potent, selective and low-calcemic inhibitors of CYP24 hydroxylase: 24-sulfoximine analogues of the hormone 1α,25-dihydroxyvitamin D_3. *J. Med. Chem*. **2004**, *47*, 6854−6863.

(20) Gomaa, M. S.; Brancale, A.; Simons, C. Homology model of 1α,25-dihydroxyvitamin D_3 24-hydroxylase cytochrome P450 24A1 (CYP24A1): active site architecture and ligand binding. *J. Steroid Biochem. Mol. Biol.* **2007**, *104*, 53–60.

(21) Zalewski, A.; Ma, N.S.; Legeza, B.; Renthal, N.; Flück, C.E.; Pandey, A.V. Vitamin D-dependent rickets type 1 caused by mutations in CYP27B1 affecting protein interactions with adrenodoxin. *J. Clin. Endocrinol. Metab*. **2016**, *101*, 3409-3418.

(22) Gasteiger, E.; Gattiker, A.; Hoogland, C.; Ivanyi, I.; Appel, R.D.; Bairoch, A. ExPASy: the proteomics server for in-depth protein knowledge and analysis. *Nucleic Acids Res*. **2003**, *31*, 3784–3788.

(23) Schaffer, A.A.; Aravind, L.; Madden, T.L.; Shavirin, S.; Spouge, J.L.; Wolf, Y.I.; Koonin, E.V.; Altschul, S.F. Improving the accuracy of PSI-BLAST protein database searches with composition- based statics and other refinements. *Nucleic acids Res.* **2001**, *29*, 2994-3005. [http://blast.ncbi.nim.hih.gov]

(24) RCSB Protein Data Bank (PDB) http://www.rcsb.org/pdb.

(25) Sievers, F.; Wilm, A.; Dineen, D.G.; Gibson, T.J.; Karplus, K.; Li, W.; Lopez, R.; McWilliam, H.; Remmert, M.; Söding, J.; Thompson, J.D.; Higgins, D.G. Fast, scalable generation of high-quality protein multiple sequence alignments using Clustal Omega. *Mol. Syst. Biol*. **2011**, *7*, 539.

(26) RAMPAGE Server http://ravenbioccam.ac.uk/rampage.php

(27) Bowie, U.J.; Eisenberg, D. Method to identify protein sequence that fold into a known three dimensional structure. *Science* **1991**, *253*, 164-170.

(28) Weiderstein, M.; Sippl, M.J. ProSA-web: interactive web service for the recognition of errors in three dimensional structures of proteins. *Nucleic Acid Res*. **2007**, *35*, 407-410.

(29) Bowers, K.J.; Chow, E.; Xu, H.; Dror, R.O.; Eastwood, M.P.; Gregersen, B.A.; Klepeis, J.L.; Kolossvary, I.; Moraes, M.A.; Sacerdoti, F.D.; Salmon, J.K.; Shan, Y.; Shaw, D.E. Scalable algorithms for molecular dynamics simulations on commodity clusters. *Proceedings of the ACM/IEEE Conference on Supercomputing (SC06), Tampa, Florida*, **2006**, November 11-17 [https://www.schrodinger.com/maestro]

(30) Molecular Operating Environment (MOE 2014.0901) Chemical Computing Group Inc, Montreal Quebec Canada http://www.chemcomp.com. 2014.0901.

(31) Zhou, Z.; Zhang, J. An efficient and green one-pot three-component synthesis of 4,4′-(arylmethylene)bis(1H-pyrazol-5-ol)s catalyzed by 2-hydroxy ethylammonium propionate. *Green Chem. Lett. Rev*. 2014, *7*, 18-23.

(32) Sobhani, S.; Nasseri, R.; Honarmand, M. 2-Hydroxyethylammonium acetate as a reusable and cost-effective ionic liquid for the efficient synthesis of bis(pyrazolyl)methanes and 2-pyrazolyl-1-nitroalkanes. *Can. J. Chem*. **2012**, *90*, 798-804.

(33) Zhu, J.; Barycki, R.; Chiellini, G.; DeLuca, H. F. Screening of selective inhibitors of 1α,25-dihydroxyvitamin D_3 24-hydroxylase using recombinant human enzyme expressed in Escherichia coli. *Biochemistry* **2010**, *49*, 10403−10411.

(34) Weiner, S.J.; Kollman, P.A.; Nguyen, D.T. An all atom forcefield for simulations of proteins and nucleic acids. *J. Comput. Chem*. **1986**, *7*, 230–252.

(35) LeadIt http://www.biosolveit.de/